ISSN (Print) 1226-1750
ISSN (Online) 2233-6656
Journal of Magnetics 27(1), 28-34 (2022) https://doi.org/10.4283/JMAG.2022.27.1.028

An Improved and Efficient Analytical Model for Magnetic Field Calculation in Linear Permanent Magnet Machines

Baocheng Guo[1], Rong Guo[2]*, Hengzai Hu[3], Jianping Shi[1], and Chunmei Feng[1]

[1]*School of Electrical and Automation Engineering, Nanjing Normal University, Nanjing 210046, China*
[2]*School of Electrical and Information Engineering, Beijing University of Civil Engineering and Architecture, Beijing 100044, China*
[3]*School of Automation, Beijing Institute of Technology, Beijing 100081, China*

(Received 23 August 2021, Received in final form 11 January 2022, Accepted 11 January 2022)

A simple and improved analytical model (AM) for linear permanent magnet synchronous machine (LPMSM) based on the correction factor is presented in this paper. A slotless linear permanent magnet machine (PLPM) with AM developed in Cartesian coordinate is selected to investigate. Consequently, the fitting equations of curvature factors for the permanent magnet and armature are obtained. The subdomains for LPMSM are simplified from 6 down to 3 domains based on curvature equations. The magnetic flux density and force show that the proposed approach agrees with the finite element (FE) model. Moreover, the reduced calculation domains and harmonic orders make AM proposed in the paper much faster. The main contribution of the work is to present a simple strategy for coordinate transformation and calculation strategy for LPMSM, which provides guideline for designers to investigate the machines developed in Cartesian coordinate.

Keywords : coordinate transformation, curvature factor, simplified sub-domain model, magnetic field

1. Introduction

Linear Permanent Magnet (LPM) machines have attracted more attention due to their compact mechanical structure and high power density [1]. They are widely used in industrial applications, such as railway transportation, renewable energy generation, and so on [2, 3]. In general, the accurate modeling of LPM requires the finite element method (FEM) [4], which is high time consuming especially in the first design stage. To reduce the duration of pre-design and improve efficiency, it is essential to choose an appropriate analytical approach.

At present, analytical calculation approaches, such as the sub-domain (SD) method [1], conformal mapping [2], etc., are preferred in initial design and optimization step. According to geometry of the machine, an analytical model can be developed and modeled in Cartesian and polar coordinates to get different solutions [3]. The movement can be divided into linear movement and rotation movement. As shown in Fig. 1(a), the machines modeled in Cartesian coordinate always move in a linear direction. Also, the machines modeled in the polar system are usually classified as a rotation movement. The rotation movement of the inner rotor machine and outer rotor machine is shown in Fig. 1(b1) and Fig. 1(b2) respectively.

A significant number of AMs have been developed for the machines modeled in different coordinates. Schwarz-Christoffel (SC) conformal mapping has been successfully applied to magnetic field calculation,which transfers the complex structure into a regular one by choosing transfer functions [4] to meet Hague's solution. In [5], the RFPM machine under eccentricity condition has been studied by authors and the SC Matlab toolbox is used to model the

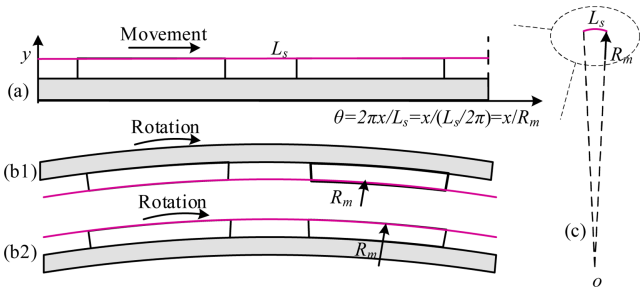

Fig. 1. (Color online) Movements of electrical machines. (a) linear movement. (b1) rotation movement for outer rotor machines. (b2) rotation movement for inner rotor machines. (c) arc movement.

*Corresponding author: Tel: +86-18813189123
Fax: +86-01061209193, e-mail: guorong@bucea.edu.cn

end effect of LPM authors in [6]. Interestingly, the SC technique is transferring the boundary conditions and calculation domains between coordinates, however, it is difficult to find suitable transfer functions when faced with a complex geometry.

Another analytical technique is the subdomain approach, which is regarded as the most accurate method since it can predict the electro-magnetic performances with good agreement. Typical coordinate transformation applications by using the SD method are presented in [7] and [8], with a sufficient long arc air region of LPM to overcome the curvature effect, which shows more calculation domains and high harmonic order in AM. For another typical machine, AFPM, authors in [9] use the correction factor to investigate the local demagnetization of PM machines, which shows the advantages of coordinate transformation. However, additional calculation models should be used to get the right factor.

It can be found from the literature that if the radius is large enough and the component moves in a sufficiently small arc line in the polar system, as shown in Fig. 1(c), anthe electrical machine moving in a limited arc line can be treated as moving in a limited straight line. For instance, the LPM in [7, 10] is converted into the polar system with a large radius, and acceptable results are obtained. However, the computation time will rise when the number of subdomains and/or the high harmonic orders from the huge solving matrix increased.

In this paper, an improved AM is developed and applied in LPM. To be specific, the curve fitting technique is used to achieve PM functions, which can consider the curve effect effectively. Afterward, the SD model for LPM is simplified and solved on the basis of previous studies. Compared to the existing literature, the transformation equation and the proposed model in this paper is simple and easy to implement, which has important guiding significance for LPM designers.

This paper is organized as follows. In Section 2, the main parameters are determined. The calculation model and curve fitting technique are shown in Section 3. SD model for LPM is simplified and developed in Section 4 based on the transformation principle. The calculation domain reduces significantly from 6 to 3. The FE model is used in Section 5 to verify the proposed model. Moreover, the experiment results are presented and compared with the results obtained from the proposed approach. Conclusions are drawn at the end of the paper.

2. Description of the Prototype

In this paper, the slotless linear PM machine in [7] is studied. The studied LPM is shown in Fig. 2. The description of the LPMSM has been shown in a previous study, so it is not repeat here.

The main parameters of the machine are illustrated in Table 1.

3. Model Developing

In this paper, the approach in [11] is used to calculate

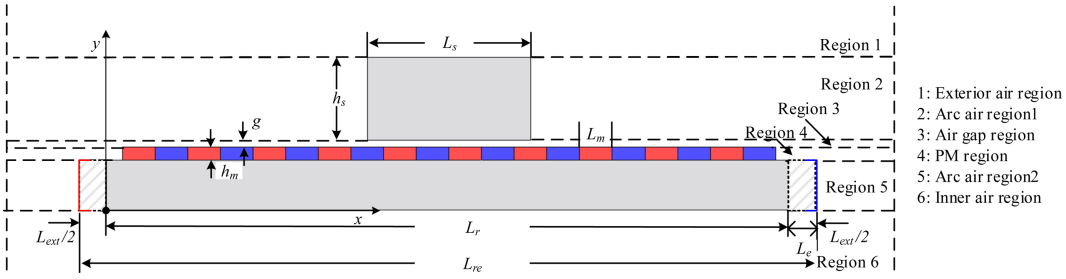

Fig. 2. (Color online) Model of the slotless LPMSM.

Table 1. Main dimensions and parameters of the LPM.

Parameter	Value	Parameter	Value
Length of primary iron, L_s	50 mm	Pole pitch, τ_p	10 mm
Height of primary iron, h_s	25 mm	Width of PM, L_m	10 mm
Length of secondary iron, L_r	210 mm	The thickness of PM, h_m	4 mm
Length of the end of secondary iron, L_e	5 mm	Pole arc to pole pitch ratio,	1.0
Axial length, L_1	50 mm	Remanence of PM, B_r	1.27T
Length of airgap, g	2 mm	Relative permeance,	1.04
Number of PMs, N_p	20	Magnetization	parallel

the magnetic induction in the air gap caused by the magnets. The following assumptions are made during calculations to reduce the complexity of the computations.

1) Magnetic material has a uniform magnetization, the relative recoil permeability μ_r is constant and the value is close to unity such as the one in NdFeB materials.

2) Magnetic saturation is absent and the rotor iron cores have infinite magnetic permeability.

3) Eddy current effects are neglected, which avoids the need for the complex eddy current field formulation.

3.1. Model Simplification

It can be seen from Fig. 1 that if the end effects are taken into consideration, 6 subdomain regions are included in the linear machine. The various region is infinite area, back-iron area, PM area, air-gap area, exterior area, and both stator and mover end areas,which will result in more unknown coefficients in the matrix. Moreover, sufficient long arc air region 2 is necessary to decrease the curvature effect and obtain acceptable results, which needs higher harmonic orders. The features make the computation time longer. The arc air region 1 can be neglected based on the previous study [7] and the proposed approach in this paper, lower harmonic orders of subdomains could be accepted because of shorter computation length. However, there are remaining 5 regions. It is well known that the smaller the number of subdomains, the shorter the CPU time, hence, the analytical model needs further simplification.

To reduce the calculation region, the approximate method in [7] is adopted in this paper. It is worthy to point out that there are different strategies to convert the coordinates. It The equivalent radius, viz., $R = L_{re}/2\pi$, is always set as the outer radius of PM or the middle of the airgap in the approximate model. When the mean air gap length is selected as the convert line, the calculation system involves the airgap length $g/2$, which is not convenient to investigate the parameters sensitive analysis. Therefore, the outer radius $R_m = R$ is selected as the covert line in the following paper.

The parameters in the polar system are calculated as:

$$\begin{cases} R_r = R_m - h_{pm} \\ R_g = R_m + g/2 \\ R_s = R_g + g/2 \\ R_{sb} = R_s + h_s \end{cases} \tag{1}$$

where R_m is the outer radius of PMs, R_r is the inner radius of PMs, R_{sb} and R_s donate the outer radius of stator and inner radius of rotor, respectively.

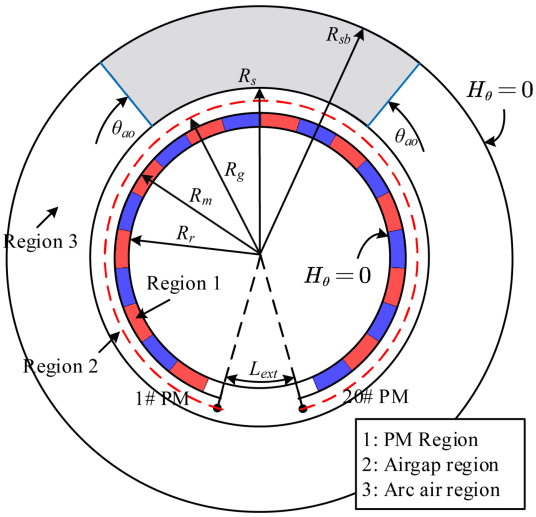

Fig. 3. (Color online) Simplified Model of the LPMSM under polar coordinate.

According to the stated in [7], the length of secondary back-iron has little influence on the magnetic field distribution and force characteristic, so it can be ignored. And based on the symmetry principle, the model in Fig. 2 can be bent into an arc structure with radius $r \to \infty$. If the length of the secondary L_{re} is finite, the radius of the simplified model in polar coordinate r will also be finite, and the secondary is rolled into a ring, Fig. 3 can be obtained.

Finally, the number of calculated subdomains can be simplified from 6 regions into 3 regions, as illustrated in Fig. 3, which will reduce the complexity and computation time significantly. It should be noted that although the length of back iron has little effect on the end effect in the model developed in Cartesian coordinate, but it may have an interaction between the adjacent PMs, 1# and 20# PMs, at the end region in the polar coordinate. To avoid the flux interactions between 1# and 20# PM in polar system, an external back iron L_{ext} is necessar y to make an "insulation space.

3.2. Model Simplification

Based on the research in [12], it can be shown that the error is mainly caused by the curvature effect. In order to obtain accurate flux densities, the correction factor is adopted in this paper.

The ratio between the magnet thickness and the average radius h_{pm}/R_{av}, which represents the curvature, is selected as the main variable. From the research, it can be found that the correct factor has little influence by the airgap length, it can be applied in LPM. More details and the curvature can be found in [12].

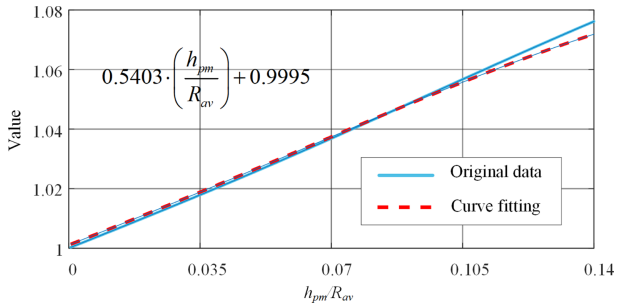

Fig. 4. (Color online) Curve effect coefficients.

The linear curve fitting technique is used here, and the correct factor function is:

$$f_B = a \cdot \left(\frac{h_{pm}}{R_{av}} \right) + b \tag{2}$$

where a and b are fitting coefficients, 0.5403 and 0.9995, respectively. The fitting formulas can meet the demand for most machines. Therefore, the flux densities under different coordinates can be transferred as:

$$B_c = f_B \cdot B_p \tag{3}$$

where B_C represents the flux densities in the Cartesian system and B_p is the results in polar coordinates.

In this paper, the extended length L_{ext} is set 20 mm and the corresponding parameters in polar coordinate are shown in Table 2.

4. Analytical Solution of Magnetic Field

4.1. Permanent Magnet Modelling

The magnetization in the tangential direction is zero for the radial magnetization. The magnetization model of permanent magnets under the mover reference coordinate system as shown in Fig. 5. The range from $N_p\theta_p$ to $\pm\pi$ is zero due to the absence of PM. Therefore, the Fourier expression of PMs should have a periodicity of 2π.

In the analytical conversion model, the magnetization

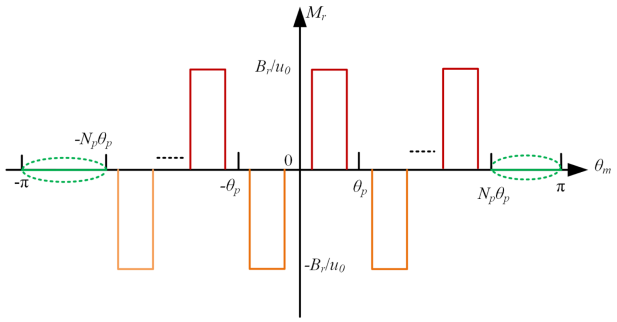

Fig. 5. (Color online) Magnetization model of PMs in radial components.

vector $\overrightarrow{M}$ of the radial and the tangential component can be defined follow [13]:

$$\begin{cases} M_r(\theta_s) = \sum_{n=1}^{\infty} M_{cnr} \cos(n\theta_s) + M_{snr} \sin(n\theta_s) \\ M_\theta(\theta_s) = \sum_{n=1}^{\infty} M_{cn\theta} \cos(n\theta_s) + M_{sn\theta} \sin(n\theta_s) \end{cases} \tag{4}$$

4.2. Model Developing

Both region I and II (PM and airgap) and slot region i and j (Slot) satisfy the Maxwell's equations. For the 2D case in polar coordinate system, by introducing magnetic vector potential, the governing function is

$$\frac{\partial^2 A}{\partial r^2} + \frac{1}{r}\frac{\partial A}{\partial r} + \frac{1}{r^2}\frac{\partial^2 A}{\partial \theta^2} = -\frac{u_0}{r}\left(M_\theta - \frac{\partial M_r}{\partial \theta_s} \right) \tag{5}$$

and

$$\frac{\partial^2 A}{\partial r^2} + \frac{1}{r}\frac{\partial A}{\partial r} + \frac{1}{r^2}\frac{\partial^2 A}{\partial \theta^2} = 0 \tag{6}$$

The scaling technique is introduced as:

$$P_\omega(u,v) = \left(\frac{u}{v}\right)^\omega + \left(\frac{v}{u}\right)^\omega, \quad E_\omega(u,v) = \left(\frac{u}{v}\right)^\omega - \left(\frac{v}{u}\right)^\omega \tag{7}$$

where u, v and w are system variables.

The general solution of vector potential A in region 1 is:

Table 2. Corresponding Parameters in Analytical Model of LPM.

Parameter	Value	Parameter	Value
Extended length, L_{ext}	20 mm	Outer radius of PM, R_m	36.6 mm
Span angle of primary iron, θ_1	78.26°	Inner radius of primary iron, R_s	38.6 mm
Outer radius of primary iron, R_{sb}	63.6 mm	Inner radius of secondary iron, R_r	32.6 mm
Axial Length, L_e	50 mm	Pole Pitch, θ_p	1.0
Span angle of PM, θ_p	15.65°	Remanence of PM, B_r	1.27T
Length of airgap, g	2 mm	Relative permeance,	1.04
Pole pitch ration, α_p	1	Magnetization	radial

$$A_1 = \left\{ \sum_{m=1}^{\infty} \left(A_m^1 \frac{P_m(r,R_r)}{P_m(R_m,R_r)} \right) \cos(m\theta) + \sum_{m=1}^{\infty} \left(C_m^1 \frac{P_m(r,R_r)}{P_m(R_m,R_r)} + M_r \right) \sin(m\theta) \right\} \tag{8}$$

The general solution in region 2 (airgap) is:

$$A_1 = \sum_{m=1}^{\infty} \left(A_m^1 \frac{P_m(r,R_s)}{E_m(R_m,R_s)} + B_m^1 \frac{P_m(r,R_m)}{E_m(R_s,R_m)} \right) \cos(m\theta) + \sum_{m=1}^{\infty} \left(C_m^1 \frac{P_m(r,R_s)}{E_m(R_m,R_s)} + D_m^1 \frac{P_m(r,R_m)}{E_m(R_s,R_m)} \right) \sin(m\theta) \tag{9}$$

The general solution in region 3 (arc air region) is:

$$A_3 = \sum_{n=1}^{\infty} \left(A_n^3 \frac{P_{n\pi/\theta_{ao}}(r,R_{sb})}{P_{n\pi/\theta_{ao}}(R_s,R_{sb})} \right) \cos\left(\frac{n\pi}{\theta_{ao}} (\theta - \theta_j) \right) \tag{10}$$

where θ_j is the center angular position of arc air, A^1_m, B^1_m, C^1_m, D^1_m and A^3_n are unknown coefficients that have to be determined. m, n are harmonic order in each computed domain.

It should be noted that each domain is connected, so the interface conditions should satisfy boundary conditions. The connections between region 1, region 2 and region 3 at R_s are:

$$\begin{cases} A_1(R_m,\theta) = A_2(R_m,\theta), \ \forall \ \theta \\ H_{\theta 1}(R_m,\theta) = H_{\theta 2}(R_m,\theta), \ \forall \theta \\ A_2(R_s,\theta) = A_3(R_s,\theta), \quad \pi - 0.5\theta_j \le \theta \le \pi + 0.5\theta_j \\ H_{\theta 2}(R_s,\theta) = H_{\theta 3}(R_s,\theta), \quad \pi - 0.5\theta_j \le \theta \le \pi + 0.5\theta_j \end{cases} \tag{11}$$

The unknown coefficients can be obtained using Fourier series expansion and boundary conditions. Afterward, the radial and tangential flux density components are calucalted as follows:

$$B_r = \frac{1}{r}\frac{\partial A}{\partial \theta}, \ B_t = -\frac{\partial A}{\partial r} \tag{12}$$

Hence, flux densities could be obtained by the superposition of each PM.

5. Validation

To verify the analytical model proposed in this paper, the FE models with linear and non-linear magnetic cores are developed by the commercial software JMAG. The semi-closed slots are applied in the model of LPMSM and the stator is located in the middle and end position,

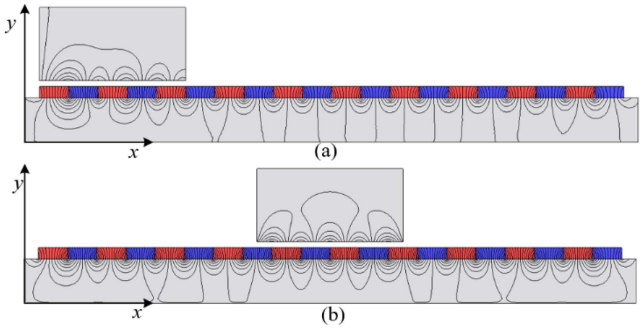

Fig. 6. (Color online) Flux lines prediction with (a) end position and (b) middle position.

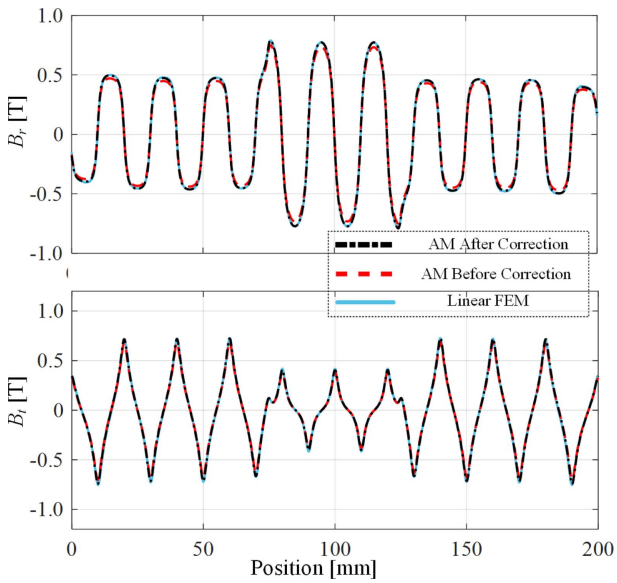

Fig. 7. (Color online) Flux lines prediction with middle position.

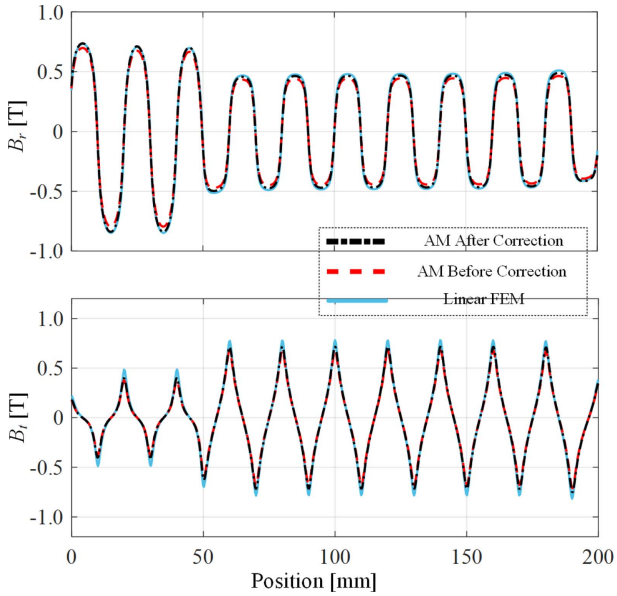

Fig. 8. (Color online) Flux lines prediction with end position.

respectively. The flux lines distribution at the typical two positions are illustrated in Fig. 6.

5.1. FE Validation

As for the analytical model, the additional back iron L_{ext} is set as 20 mm to avoid interaction between the PMs at the end position. The harmonic order m and n are both set as 200, due to the relatively large slot region.

According to the Maxwell tensor equation, the cogging torque of radial model can be computed as follows

$$F_{\mathrm{d}}=\frac{1}{\mu_0}L\int_0^{2\pi}B_{r2}(r,\theta)B_{\theta 2}(r,\theta)rd\theta \tag{13}$$

where L is axial length, R_{av} is the average radius of air gap.

With regards to the LPMSM, the thrust force is one of the main performances of the machine. According to the lever principle, the thrust force can be converted as mentioned in [14]:

$$F_t=\frac{L}{u_0}\int_{-\tau}^{\tau}B_x^{II}B_y^{II}dx \tag{14}$$

The slotless PM prototype and experiment platform are shown in Fig. 9:

The force sensor is used to detect the detent force, the full scale is 98 N and precision of 0.2% which is enough to measurement. The relative position between the stator and mover is measured by a vernier caliper with precision of 0.02 mm. The data is recorded by force sensor meter.

Figure 10 shows the comparison of detent force. It can be seen that the proposed model can predict the force with acceptable accuracy and the waveforms are quite similar. There is some slight discrepancy, this may be caused by two reasons, one is the curvature effect for tangential component, another is the simplifications in the proposed model. However, despite that, the proposed model in this paper is accurate enough to use in the design and optimization stage.

5.2. Comparison

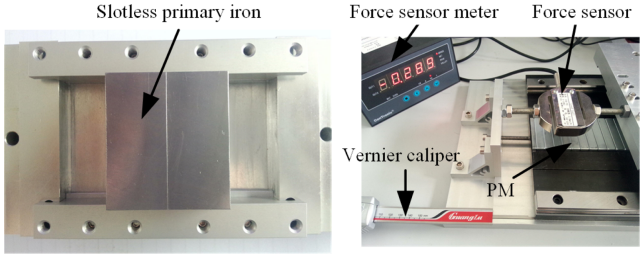

Fig. 9. (Color online) Slotless Prototype and experiment platform.

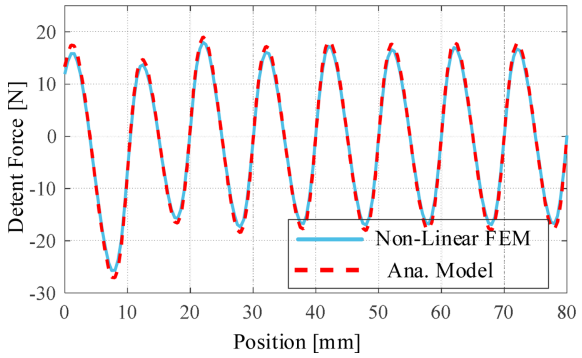

Fig. 10. (Color online) Detent force comparison between FEM and AM.

To futher verify the proposed model, the prototype is manufactured and an experiment platform is built-in [7]. the detent force is compared with the experimental results, as shown in Fig. 10. It shows that the force corresponds very well with the results of the proposed model in this paper, verifing the validity of the proposed analytical model.

The CPU time between the FEM and analytical model is also compared by a core i7 processor and 16 GB installed memory with 64bit operating Windows 10 system.

The computation time is as shown in Table 3. FE model calculates the magnetic properties of an electrical cycle in about 2 minutes. Compared with existing literature [7], the magnetic properties of LPMSM with an extended arc air region of 2000 mm are calculated in 20 seconds without considering the slots.As for the model presents in this paper, only 4 sec is needed, it takes much less CPU

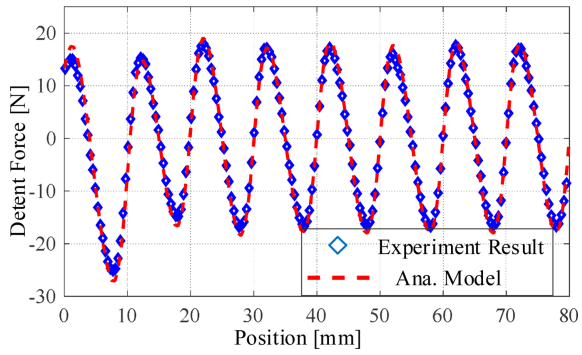

Fig. 11. (Color online) Detent force comparison between experiment and AM.

Table 3. Comparison between different methods.

	Linear FEM	Model in [7]	Proposed model
Time	1 min58 sec	20 sec	1.6 sec
RMS Force	12.34 N	12.44 N	13.22 N

time than the existing analytical approach.

Although a similar error exists when comparing analytical results to experimental values, it is still acceptable and thus, it can be regarded as a meaningful approach that could save time and achieve an acceptable result.

6. Conclusion

This paper presents an improved analytical model to evaluate the magnetic field and forces of the linear PM machine. The model is developed based on the approximate approach, which rolling the LPM into a rotary machine. In this model, we introduce a correction factor by curve fitting technique, and this factor can obtain the high accuracy results with relatively small extended arc air region. The results show that the magnetic flux densities matched well and so does the detent force. The FEM and experiments are both conducted.

The CPU time is reduced while maintains the accuracy. The model in this paper can deal with the slotted LPM machine, which will be done in the following research.

Acknowledgment

This work was supported in part by the National Nature Science Foundation of China under Grant 51907027, and in part by BUCEA Young Scholar Research Capability Improvement Plan under Grant X21081. This work was supported in part by the National Nature Science Foundation of China under Grant 51907027, Jiangsu Provincinal Grant JSSCBC20210306, and in part by BUCEA Young Scholar Research Capability Improvement Plan under Grant X21081.

References

[1] L. J. Wu, Z. Q. Zhu, D. Staton, M. Popescu, and D. Hawkins, IEEE Trans. Magn. **47**, 1693 (2011).
[2] B. Guo, Y. Huang, F. Peng, and J. Dong, IEEE Trans. Ind. Electron. **66**, 5015 (2019).
[3] B. L. J. Gysen, K. J. Meessen, J. J. H. Paulides, and E. A. Lomonova, IEEE Trans. Magn. **46**, 39 (2010).
[4] T. A. Driscoll and L. N. Trefethen, Schwarz-Christoffel mapping. Cambridge; New York: Cambridge University Press, 2002.
[5] F. R. Alam and K. Abbaszadeh, IEEE Trans. Energy Convers. **31**, 333 (2015).
[6] L. Zeng, X. Chen, X. Li, W. Jiang, and X. Luo, IEEE Trans. Magn. **51**, 1 (2015).
[7] H. Hu, J. Zhao, X. Liu, and Y. Guo, IEEE Trans. Ind. Electron. **63**, 7632 (2016).
[8] H. Hu, J. Zhao, X. Liu, Y. Guo, and J. Zhu, IEEE Trans. Ind. Electron. **64**, 5564 (2017).
[9] B. Guo, Y. Huang, F. Peng, and J. Dong, IEEE Trans. Ind. Electron. **66**, 5830 (2019).
[10] H. Hu, X. Liu, J. Zhao, and Y. Guo, IEEE Trans. Ind. Electron. **65**, 2475 (2018).
[11] A. Hemeida and P. Sergeant, IEEE Trans. Magn. **50**, 1 (2014).
[12] B. Guo, Y. Huang, F. Peng, J. Dong, and Y. Li, IEEE Trans. Ind. Electron. **67**, 4433 (2020).
[13] R. Guo, H. Yu, Y. Kong, T. Xia, X. Liu, and Z. Wu, IEEE Trans. Magn. **54**, 1 (2018).
[14] K.-H. Shin, K.-H. Kim, K. Hong, and J.-Y. Choi, IEEE Trans. Magn. **53**, 1 (2017).